Triphenyl phosphate is a selective PPARγ modulator that does not induce brite adipogenesis *in vitro* and *in vivo*

Stephanie Kim,[1,2] Nabil Rabhi,[3] Benjamin C. Blum,[4] Ryan Hekman,[4] Kieran Wynne,[4] Andrew Emili,[4] Stephen Farmer,[3] Jennifer J. Schlezinger[1,2]

[1]Boston University Superfund Research Program, Boston University, MA 02118 USA
[2]Boston University School of Public Health, Department of Environmental Health, MA 02118 USA
[3]Boston University School of Medicine, Department of Biochemistry, MA 02118 USA
[4]Boston University School of Medicine, Center for Network Systems Biology, MA 02118 USA

Corresponding author:
Jennifer J. Schlezinger, Ph.D.
Boston University School of Public Health
Dept. of Environmental Health
715 Albany Street, R-405
Boston, MA 02118
Phone: 617-638-6497
Email: jschlezi@bu.edu

Declaration of competing financial interests (CFI):

The authors declare they have no actual or potential competing financial interests.

Grant Information:

Superfund Research Program [P42 ES007381]

NIH/NIDDK {R01 DK117161]

Abstract:

Background: Triphenyl phosphate (TPhP) is an environmental PPARγ ligand, and growing evidence suggests that it is a metabolic disruptor. We have shown previously that the structurally similar ligand, tributyltin, does not induce brite adipocyte gene expression.

Objectives: First, we tested whether TPhP also fails to induce brite adipogenesis *in vivo*, in human primary preadipocytes and in 3T3 L1 cells. Second, we tested the hypothesis that TPhP is a selective PPARγ modulator that is unable to protect PPARγ from phosphorylation at serine 273.

Methods: C57BL/6J male mice were fed either a low or very high fat diet for 13 weeks. From weeks 7-13, mice were injected intraperitoneally, daily, with vehicle, rosiglitazone (Rosi), or TPhP (10 mg/kg). Mature adipocytes were isolated from inguinal adipose tissue to assess adipocyte gene expression. Adipocyte genotype and phenotype were assessed in human primary preadipocytes differentiated in the presence of Rosi, or TPhP. Adipocyte gene and protein expression were determined in 3T3 L1 cells differentiated in the presence of Rosi or TPhP. Swiss 3T3 cell lines expressing wild-type PPARγ2 or PPARγ2 with alanine substitute for serine at position 273 were used to determine effects of PPARγ phosphorylation on Rosi- and TPhP-induced gene expression.

Results: Compared to Rosi**,** TPhP did not induce browning of mature adipocytes. TPhP also did not induce expression of brite adipocyte genes, mitochondrial biogenesis or cellular respiration in primary human adipocytes. Rosi and TPhP induced distinct proteomic and phosphoproteomic profiles; Rosi enriched more regulatory pathways related to fatty acid oxidation and mitochondrial proteins. Furthermore, TPhP maintained phosphorylation of PPARγ at ser273. Upon inhibition of phosphorylation at ser273, TPhP was able to induce brite adipocyte genes.

Discussion: Here, we show that TPhP acts via a novel mechanism of action. TPhP disrupts brite adipocyte differentiation by failing to protect PPARγ from phosphorylation at ser273, in contrast to the therapeutic PPARγ ligand Rosi.

Introduction:

The Endocrine Society's latest scientific statement on the obesity pathogenesis states that obesity is a disorder of the energy homeostasis system, rather than just a passive accumulation of adipose, and that environmental factors, including chemicals, confer obesity risk (Schwartz et al. 2017). This coincides with the Metabolism Disrupting Chemical (MDC) hypothesis, which proposes that environmental chemicals " promote metabolic changes that can result in obesity, type 2 diabetes or fatty liver in animals including humans; these metabolic alterations may play an important role in the global epidemics of obesity, type 2 diabetes and metabolic syndrome" (Heindel et al. 2017). This hypothesis is not without controversy, in part, because many MDCs are ligands for PPARγ, a therapeutic target for treatment of type 2 diabetes.

One class of chemicals that are suspected MDCs are organophosphate esters (OPEs). These chemicals are extensively used as flame retardants and plasticizers in consumer products from furniture to nail polish (Mendelsohn et al. 2016; Wang et al. 2019). An analysis of 2,666 urine samples from the 2013-14 National Health and Nutrition Examination Survey for biomarkers of organophosphate flame retardant exposure showed that exposure to triphenyl phosphate (TPhP) and tris(1,3-dichloro-2-propyl) phosphate are nearly ubiquitous in Americans (92% detection frequency) (Ospina et al. 2018). Several studies have evaluated the metabolic effects of early life exposures to TPhP in adults. Perinatal TPhP exposure increased body and fat mass in 3.5 month old male and female rats and increased fasting plasma non-esterified-fatty acids in the male rats (Green et al. 2016). Perinatal TPhP exposure in male mice resulted in increased body weight, liver weight, lipid-related metabolites, and fat mass and suppressed pyruvate metabolism and tricarboxylic acid cycles in adults (Wang et al. 2018). There is also evidence of impaired glucose homeostasis in adults following early life exposures to TPhP (Green et al. 2016; Patisaul et al. 2013; Wang et al. 2018).

OPEs and their metabolites are ligands for multiple human nuclear receptors (Kojima et al. 2013, 2016). There is strong evidence that TPhP is a peroxisome proliferator-activated receptor γ (PPARγ) ligand and is adipogenic (Belcher et al. 2014; Fang et al. 2015; Pillai et al. 2014; Tung et al. 2017a, 2017b). TPhP induced lipid accumulation and perilipin (lipid droplet marker) protein expression in mouse BMS2 cells and increased adipocyte protein 2 (*aP2*) mRNA expression in mouse 3T3-L1 adipocytes (Pillai et al. 2014; Tung et al. 2017a). TPhP induced lipid accumulation and increased *FABP4* and *LPL* mRNA expression in human preadipocytes (Tung et al. 2017b).

PPARγ is required for adipocyte differentiation, regulation of insulin sensitivity, and in regulating the molecular events that generate white, brown, and brite (brown-in-white) adipocytes (Lefterova et al. 2014; Ma et al. 2018). White adipocytes are characterized by a single large lipid droplet and store excess energy in forms of triglycerides (Ma et al. 2018). Brown adipocytes contain multiple, small lipid droplets and have a high density of mitochondria. A high level of expression of Ucp1 in brown adipocytes uncouples the electron transport chain from synthesis of ATP resulting in heat production and high energy expenditure. Brown adipocytes play an important role in thermogenesis (Ma et al. 2018). The more recently discovered brite adipocytes are of white adipocyte origin, but have smaller, multi-locular lipid droplets and a higher mitochondrial density than white adipocytes (Chen et al. 2016; Ma et al. 2018). The ability of PPARγ to induce the differentiation and control the function of both white and brown adipocytes results from a fine tuning of its transcriptional repertoire by post-translational modification and recruitment of coregulators (Kim et al. 2013).

PPARγ can be regulated by post-translational modifications such as phosphorylation (Burns and Vanden Heuvel 2007). Phosphorylation of PPARγ on ser112 in the N-terminal A/B domain

inhibits ligand binding, but reduced phosphorylation at ser112 is associated with increased adiposity (Rangwala et al. 2003; Shao et al. 1998). PPARγ also can be phosphorylated by cyclin-dependent kinase 5 (Cdk5) on ser273 in the ligand-binding domain, whic dysregulates the expression of genes involved in insulin-sensitization including adipsin and adiponectin (Choi et al. 2010). PPARγ ligands, such as rosiglitazone (an anti-diabetic therapeutic), that are capable of inhibiting phosphorylation at ser273 improve glycemic control and insulin sensitivity (Banks et al. 2015; Choi et al. 2010; Ma et al. 2018). These healthful metabolic effects can be mimicked by a Cdk5 inhibitor, roscovitine (Wang et al. 2016). Thus, it has been suggested that PPARγ agonism is not a prerequisite for the beneficial effects of inhibited phosphorylation at ser273 (Choi et al. 2011). Moreover, ser273 of PPARγ is in close proximity with the RXRα DNA binding domain, implicating protein-protein interactions and resulting dynamics as a target for phosphorylation that can ultimately regulate the recruitment of coregulators (Chandra et al. 2008; Lemkul et al. 2015). Indeed, selective PPARγ activation is a strategy being used to design therapeutics that maximize insulin sensitization while minimizing adverse effects (Garcia-Vallvé et al. 2015).

We have previously shown that tributyltin (TBT) acts through PPARγ to enhance adipocyte differentiation but is not able to induce health-promoting activities of PPARγ such as mitochondrial biogenesis and cellular respiration (Kim et al. 2018). Yet, it is unclear how environmental MDCs act disparately from therapeutic PPARγ ligands . Here, we investigate the hypothesis that TPhP is a selective PPARγ modulator that fails to protect PPARγ from phosphorylation at ser273. We began by testing TPhP's ability to induce brite adipogenesis in vivo, in primary human pre-adipocytes. Then, we used the 3T3 L1 model and 3T3 cells expressing wildtype and mutant PPARγ to investigate the role of PPARγ phosphorylation in the disparate effects of TPhP and rosiglitazone on adipocyte differentiation. Overall, the results support the conclusion that TPhP is a selective PPARγ modulator.

Methods:

Chemicals

DMSO was purchased from American Bioanalytical (Natick, MA). Cell culture chemicals were from Sigma-Aldrich (St. Louis, MO). Rosiglitazone (cat. #71740, purity ≥ 98%) was from Cayman Chemical (Ann Arbor, MI). Roscovitine (#R7772, purity ≥ 98%) and triphenyl phosphate (cat. #241288, purity ≥ 99%) were from Sigma-Aldrich. All other reagents were from Thermo Fisher Scientific (Waltham, MA), unless noted.

In-vivo experiments

Six-week-old, male C57BL/6J mice (DIO, Stock No: 380050 and DIO Control, Stock No: 380056) were obtained from Jackson Laboratory (Bar Harbor, ME) and housed at 23°C in a 12 hr light/dark cycle. Experimental procedures were approved by the Boston University Institutional Animal Care and Use Committee and performed in an American Association for the Accreditation of Laboratory Animal Care accredited facility (Animal Welfare Assurance Number: A3316-01). Water and food were provided *ad libitum*. Mice were fed either a diet with 60% kcal% fat (high fat diet, D12492, Research Diets, New Brunswick, NJ) or 10% kcal% fat (low fat diet, D12450B, Research Diets) for a total of 13 weeks. Seven weeks after initiation of the diet, mice were injected intraperitoneally (i.p.), daily for 6 weeks with vehicle (composition: 50% saline, 45% PG400, and 5% TWEEN 80; volume was calculated depending on the mouse weight), rosiglitazone (Rosi, 10 mg/kg), or triphenyl phosphate (TPhP, 10 mg/kg). Mice were weighed daily. Body composition was measured by noninvasive quantitative MRI (EchoMRI700) before euthanasia. To isolate mature adipocytes (MA), inguinal white adipose tissue (IWAT) was minced, resuspended in 5 ml 1% collagenase type II in DMEM with 2.5% BSA and

incubated, rocking for 40 min at 37°C. Samples were filtered through 100 and 40 µm strainers (BD Bioscience), and centrifuged for 10 min at 500 × rpm (pellet fraction were mature adipocytes). For immunohistochemistry, IWAT was fixed in 4% formalin, paraffin-embedded, sectioned (5 µm) and stained with hematoxylin and eosin (Rabhi et al. 2018). Adipocyte size and number were measured using ImageJ software (Schneider et al. 2012).

Cell Culture

NIH 3T3-L1 (ATCC: CL-173, RRID:CVCL_0123, Lot # 63343749), 3T3-PPARγ WT and 3T3-PPARγ S273A cells (Qiang et al. 2012) were maintained in high-glucose DMEM with 10% calf serum, 100 U/ml penicillin, 100 µg/ml streptomycin, 0.25 µg/ml amphotericin B. All experiments with 3T3-L1 cells were conducted with passages 3-8. Cells were plated in maintenance medium and incubated for 3 days. “Naïve” cells were cultured in maintenance medium for the duration of an experiment. On day 0, differentiation was induced by replacing the maintenance medium with DMEM containing 10% fetal bovine serum (FBS, Sigma-Aldrich), 250 nM dexamethasone, 167 nM of 1 µg/ml human insulin, 0.5 mM IBMX, 100 U/ml penicillin, and 100 µg/ml streptomycin. On days 3 and 5 of differentiation, medium was replaced with adipocyte maintenance medium (DMEM, 10% FBS, 167 nM human insulin, 100 U/ml penicillin, 100 µg/ml streptomycin), and the cultures were dosed with vehicle (DMSO, 0.1% final concentration), Rosi (20uM), or TPhP (20uM). On Day 7 of differentiation, medium was replaced with adipocyte medium (DMEM, 10% FBS, 100 U/ml penicillin, 100 µg/ml streptomycin), and the cultures were re-dosed. For CDK5 inhibition experiments, cells were treated with Vh or roscovitine (Rosco, 20 µM) at the initiation of differentiation as well as on days 3, 5, and 7 of differentiation. For PPARγ antagonist experiments, cells were treated with Vh or T0070907 (20 µM) at the initiation of differentiation as well as on days 3, 4, 5 and 6 of differentiation. Following 10 days of differentiation and dosing, cells were harvested for cell number analyses (JANUS staining), gene expression, proteome expression, lipid accumulation, mitochondrial biogenesis, and cellular respiration analyses.

Primary, human, subcutaneous pre-adipocytes were obtained from the Boston Nutrition Obesity Research Center (Boston, MA). Pre-adipocytes were maintained in αMEM with 10% FBS, 100 U/ml penicillin, 100 µg/ml streptomycin, 0.25 µg/ml amphotericin B. Pre-adipocytes were plated in maintenance medium and incubated for 3 days. “Naïve” cells were cultured in maintenance medium for the duration of the experiment. On day 0, differentiation was induced by replacing the maintenance medium with DMEM/F12, 25 mM $NaHCO_3$, 100 U/ml penicillin, 100 µg/ml streptomycin, 33 µM d-Biotin, 17 µM pantothenate, 100 nM dexamethasone, 100 nM human insulin, 0.5 mM IBMX, 2 nM T_3, and 10 µg/ml transferrin. Experimental wells received induction medium and were treated with vehicle (DMSO, 0.1% final concentration), Rosi (4µM), or TPhP (4µM). On day 3 of differentiation, medium was replaced with induction medium, and the cultures were re-dosed. On days 5, 7, 10, and 12 of differentiation, the medium was replaced with adipocyte medium (DMEM/F12, 25 mM $NaHCO_3$, 100 U/ml penicillin, 100 µg/ml streptomycin, 33 µM d-Biotin, 17 µM pantothenate, 10 nM dexamethasone, 10 nM insulin, and 3% bovine calf serum) and the cultures were re-dosed. Following 14 days of differentiation and dosing, cells were harvested for cell number analyses (JANUS staining), gene expression, lipid accumulation, fatty acid uptake, mitochondrial biogenesis, and cellular respiration analyses.

Reverse Transcriptase (RT)-qPCR

Total RNA was extracted and genomic DNA was removed using the Direct-zol 96-well MagBead RNA Kit (Zymo Research, Orange, CA). cDNA was synthesized from total RNA using the iScript™ Reverse Transcription System (BioRad, Hercules, CA). All qPCR reactions were performed using PowerUp™ SYBR Green Master Mix (Thermo Fisher Scientific, Waltham, MA). The qPCR reactions were performed using a 7500 Fast Real-Time PCR System (Applied

Biosystems, Carlsbad, CA): UDG activation (50°C for 2 min), polymerase activation (95°C for 2 min), 40 cycles of denaturation (95°C for 15 sec) and annealing (various temperatures for 15 sec), extension (72°C for 60 sec). The primer sequences and annealing temperatures are provided in Table S1. Relative gene expression was determined using the Pfaffl method to account for differential primer efficiencies (Pfaffl 2001), using the geometric mean of the Cq values for beta-2-microglobulin (*B2m*) and 18s ribosomal RNA (*Rn18s*) for mouse gene normalization and of ribosomal protein L27 (*RPL27*) and *B2M* for human gene normalization. The Cq value from naïve, undifferentiated cultures was used as the reference point. Data are reported as "Relative Expression" compared to vehicle (Vh, 0.1%DMSO) for *in-vitro* experiments and compared to vehicle of low-fat or high-fat diet group for *in-vivo* experiments.

Lipid Accumulation

3T3-L1 cells or human preadipocytes were plated in 24 well plates at 50,000 cells per well in 0.5 ml maintenance medium at initiation of the experiment. Medium was removed from the differentiated cells, and they were rinsed with PBS. The cells were then incubated with Nile Red (1 µg/ml in PBS) for 15 min in the dark. Fluorescence (λex= 485 nm, λem= 530 nm) was measured using a Synergy2 plate reader (BioTek Inc., Winooski, VT). The fluorescence in all control and experimental wells was normalized by subtracting the fluorescence measured in naïve (undifferentiated) cells. The naïve-corrected fluorescence in the experimental wells was divided by the naïve-corrected fluorescence in the rosiglitazone wells and reported as "% Maximum Lipid Accumulation."

Cell Death

3T3-L1 cells or human preadipocytes were plated in 96 well, black-sided plates at 10,000 cells per well in 0.2 ml maintenance medium at initiation of the experiment. Cells death was measured by treating differentiated cells will MitoOrange Dye according to manufacturer's protocol (Abcam, Cambridge, MA). Measurement of fluorescence intensity (λex= 485 nm, λem= 530 nm) was performed using a Synergy2 plate reader. The fluorescence in experimental wells was normalized by subtracting the fluorescence measured in naïve (undifferentiated) cells and reported as "RFUs."

Fatty Acid Uptake

3T3-L1 cells or human preadipocytes were plated in 96 well, black-sided plates at 10,000 cells per well in 0.2 ml maintenance medium at initiation of the experiment. Fatty acid uptake was measured by treating differentiated cells with 100 µL of Fatty Acid Dye Loading Solution (Sigma-Aldrich, MAK156). Following a 1 hr incubation, measurement of fluorescence intensity (λex= 485nm, λem= 530nm) was performed using a Synergy2 plate reader. The fluorescence in experimental wells was normalized by subtracting the fluorescence measured in naïve (undifferentiated) cells and reported as fold difference from vehicle "RFUs."

Mitochondrial Biogenesis

3T3-L1 cells or human preadipocytes were plated in 24 well plates at 50,000 cells per well in 0.5 ml maintenance medium at initiation of the experiment. Mitochondrial biogenesis was measured in differentiated cells using the MitoBiogenesis In-Cell Elisa Colorimetric Kit, following the manufacturer's protocol (Abcam). The expression of two mitochondrial proteins (COX1 and SDH) were measured simultaneously and normalized to the total protein content via JANUS staining. Absorbance (OD 600nm for COX1, OD 405nm for SDH, and OD 595nm for JANUS) was measured using a BioTek Synergy2 plate reader. The absorbance ratios of COX/SDH in experimental wells were normalized to the naïve (undifferentiated) cells.

Oxygen Consumption

3T3-L1 cells or human preadipocytes were plated in Agilent Seahorse plates at a density of 50,000 cells per well in 0.5 ml maintenance medium at initiation of the experiment. Prior to all assays, cell media was changed to Seahorse XF Assay Medium without glucose (1mM sodium pyruvate, 1mM GlutaMax, pH 7.4) and incubated at 37°C in a non-CO_2 incubator for 30 min. To measure mitochondrial respiration, the Agilent Seahorse XF96 Cell Mito Stress Test Analyzer (available at BUMC Analytical Instrumentation Core) was used, following the manufacturer's standard protocol. The compounds and their concentrations used to determine oxygen consumption rate (OCR) included 1) 0.5 μM oligomycin, 1.0 μM carbonyl cyanide-p-trifluoromethoxyphenylhydrazone (FCCP) and 2 μM rotenone for 3T3-L1s; and 2) 5 μM oligomycin, 2.5 μM FCCP, and 10 μM rotenone for the primary human adipocytes.

Immunoblot Analyses

3T3-L1 cells were plated in 6-well plates at 200,000 cells per well in 2 ml maintenance medium at initiation of the experiment. Cells were lysed in RIPA Buffer with PMSF (Cell Signaling Technology, Danvers, MA). Proteins (50 ug) were fractionated using SDS-PAGE on 10% Mini-PROTEAN TGX protein gels (Bio-Rad) and were transferred to nitrocellulose membranes (Bio-Rad). Following transfer, the membranes were blocked with 5% bovine serum albumin in phosphate-buffered saline-0.1% Tween 20 and probed with rabbit anti-PPARγ antibody (#2443S, Cell Signaling Technology) and phospho-ser273 PPARγ (bs-4888R, Bioss, Woburn, MA). Immunoreactive bands were detected using HRP-conjugated secondary antibodies (Biorad) followed by enhanced chemiluminescence.

Proteomic Analyses

3T3-L1 cells were plated in T75 flasks at 1,000,000 cells per well in 10 ml maintenance medium at initiation of the experiment. Cells were re-suspended in 8M Urea/50mM triethylammonium bicarbonate (TEAB), with phosphatase and protease inhibitors (Roche, Basel, CH) then sonicated (3x10 seconds) on ice. Samples were reduced for 30 minutes with 8 mM dithiothreitol and alkylated for 15 minutes with 20mM iodoacetamide at 30°C. The 8M urea solution was diluted to 1M with 50 mM TEAB, and samples were digested overnight at 37°C with 20 μg sequencing grade trypsin (90057, Thermo Fisher Scientific).

Prior to TMT (Tandem Mass Tag) labeling, peptides were extracted from each sample using c18 spin columns (Toptip, Glygen, Columbia, MD), and peptide concentrations were normalized to 100ug in 100ul of 100mM TEAB. Peptides were labelled with 0.8 mg of TMT label (TMT10plex™ Isobaric Label Reagent Set, Thermo Fisher Scientific). Labelled samples were pooled, and 95% was set aside for phospho-peptide enrichment using TiO_2 (Titansphere Phos-TiO Bulk 10 um, GL Sciences, Tokyo, JP) (Cantin et al. 2007). The remaining 5% of labelled peptides and the phospho-peptide enriched samples were analyzed separately by mass spectrometry.

Samples were analyzed on a Q Exactive HFX mass spectrometer connected to an Easy nLC 1200 chromatography system (Thermo Fisher Scientific). Peptides were re-suspended in 0.1% formic acid. Each sample was loaded onto a nano-trap column (75μm i.d. × 2 cm, Acclaim PepMap100 C18 3μm, 100Å, Thermo Fisher Scientific) with mobile phase A (97.9% water, 2% acetonitrile, 0.1% formic acid) and resolved with an increasing mobile phase B (80% acetonitrile, 19.9% water, 0.1% formic acid) over an EASY-Spray column, (50 cm × 75 μm ID, PepMap RSLC C18, Thermo Fisher Scientific) for 180 minutes at a flow rate of 250 nL/min The mass spectrometer was operated in positive ion mode with a capillary temperature of 300°C, and with a potential of 2100V applied to the frit. All data was acquired with the mass spectrometer operating in automatic data dependent switching mode. A high resolution (60,000)

MS scan (350-1500 m/z) was performed using the Q Exactive to select the 10 most intense ions prior to MS/MS analysis using HCD (NCE 33, 45,000 resolution).

Resulting RAW files were searched using MaxQuant (version 1.6.0; www.coxdocs.org/doku.php?id=maxquant:start) under standard settings using the UniProt mouse database (downloaded October 2018, www.uniprot.org/taxonomy/10090) allowing for two missed trypsin cleavage sites and variable modifications of N-terminal acetylation and methionine oxidation (Tyanova et al. 2016). Additionally, protein phosphorylation at S, T, and Y residues were included as variable modifications in the phosphoproteomics data. Carbamidomethylation of cysteine residues was a fixed modification in the search. Candidate (phospho)peptides, proteins, and phosphorylation-site identifications were filtered based on a 1% false discovery rate threshold based on searching the reverse sequence database. Data are deposited and publicly available at the PRIDE archive. All phosphopeptide identifications in the MaxQuant evidence file had to meet a 0.7 probability cutoff.

The searched intensity data were filtered, normalized, and clustered using R [https://www.R-project.org/]. Feature filtering was performed to remove any feature in less than 70 percent of samples with 1627 proteins and 1066 phospho-sites passing the filter in the proteomics and phosphoproteomic data sets, respectively. The LIMMA R package was used for LOESS normalization and differential expression analysis (Ritchie et al. 2015). A combined ranked list for both sets was generated where duplicate gene entries were removed to keep the entry with the highest absolute rank value.

Gene Set Enrichment Analysis (GSEA) software from the Broad Institute (software.broadinstitute.org/GSEA)(version 3.0) was used in rank mode along with gene sets downloaded from the Bader Lab (Mouse_GOBP_AllPathways_no_GO_iea_October_01_2018_symbol.gmt) from http://baderlab.org/GeneSets) (Merico et al. 2010; Subramanian et al. 2005). GSEA results were visualized using the Enrichment Map app (Version 3.1) in Cytoscape (Version 3.6.1) and highly related pathways were grouped into a theme and labeled by AutoAnnotate (version 1.2). For the merged gene set analyses, we applied an enrichment $P < 0.01$ and FDR ≤ 0.1 cutoff and calculated overlap between gene set annotations using a combination of Jaccard and overlap coefficients with a cutoff of 0.375.

Statistical Analyses and Publicly Available Data

All statistical analyses were performed in R (v 3.5.0) and Prism 7 (GraphPad Software, Inc., La Jolla, CA). Data are presented as means $\pm$ standard error (SE). For 3T3-L1 experiments the biological replicate is an independently plated experiment. For human primary preadipocyte experiments, the biological replicate is a single individual's preadipocytes (3 individuals in all). The qPCR data were log-transformed before statistical analyses. One-factor ANOVAs (Dunnett's) were performed to analyze the qPCR and phenotypic data. The mass spectrometry proteomics and phosphoproteomics data are available from PRIDE (http://www.proteomexchange.org) under accession number PXD012337.

Results:

Effect of TPhP on adipocyte browning in vivo

We examined *in-vivo* effects of Rosi and TPhP exposure in six-week-old C57BL/6J male mice that were also fed either low fat diet (LFD) or high fat diet (HFD). We chose male mice as C57BL/6 male mice are more likely to become obese than female mice, and it has been suggested that male mice are more vulnerable than the females to the impacts of HFD on weight gain and metabolic disruption (Hong et al. 2009; Hwang et al. 2010). Compared to Vh-

treated mice on LFD, small but not significant increases in body weight were observed in mice that were exposed to Rosi or TPhP (**Figure S1A**). Generally, the body weights of HFD mice were greater than LFD mice exposed to Vh. Body weights, as well as fat mass, in Rosi- and TPhP- treated mice on HFD were lower than that of Vh-treated mice on HFD (**Figures S1A-B**). There were no significant differences in lean mass (**Figure S1B**).

In inguinal white adipose tissue (IWAT), white adipocytes can attain a brown-like phenotype and express thermogenic genes (Kalinovich et al. 2017; Paschos et al. 2018). Rosi and TPhP increased the number of adipocytes in IWAT of mice fed either a high or low fat diet and significantly decreased the size of these adipocytes in both diet groups (**Figures 1A-B**). We measured expression of white adipocyte genes (*Fabp4, Plin1, Cidec, Retn*, and *Wdnm1*) and brite adipocyte genes (*Adipoq*, *Cidea*, *Elovl3*, *Ucp1*, *Acaa2*, *CoxIV*) in mature adipocytes (MA) of the IWAT. Rosi and TPhP did not change the expression of *Fabp4* but significantly induced expression of *Plin1* and *Cidec,* proteins associated with lipid droplets, in both diet groups (**Figure 1C**). TPhP increased *Retn* expression in both diet groups, while Rosi increased its expression only in the HFD group (**Figure 1C**). Rosi only significantly reduced *Wdnm1* expression in the LFD group (**Figure 1C**). In the LFD group, Rosi only significantly induced expression of known markers of brite adipocytes; while TPhP significantly reduced expression of *Elovl3* and*Ucp1* and also reduced *Acaa2* expression (**Figure 1D**). In the HFD group, Rosi significantly induced expression of *Elovl3, Cidea, Acaa2,* and *CoxIV*; while TPhP significantly increased only *Acaa2* expression (**Figure 1E**). Moreover, in the HFD group, TPhP significantly reduced expression of *Elovl3* and *Ucp1* (**Figure 1D**). Hence, *in-vivo* TPhP exposure did not significantly induce browning of white adipose tissue.

Effect of TPhP on differentiation of human adipocytes

Primary human adipocytes were differentiated using a standard hormone cocktail for a total of 14 days. During differentiation, cells were treated with vehicle (0.1% DMSO, final concentration), Rosi (4 μM), or TPhP (4 μM). Both Rosi and TPhP significantly increased cell number (**Figure S2A**) and significantly induced lipid accumulation (**Figure 2A**). However, only Rosi significantly induced fatty acid uptake, mitochondrial biogenesis, and cellular respiration in differentiated primary human adipocytes (**Figures 2B-D**). Both Rosi and TPhP significantly increased expression of *PPARG* and expression of the white adipocyte genes, *PLIN1, CIDEC,* and *FABP4* (**Figure 2E**). While both Rosi and TPhP significantly induced the energy expenditure gene, *ACAA2*, only Rosi significantly increased expression of browning markers, *ELOVL3*, *CIDEA* and *UCP1* (**Figure 2E**). These observations in primary human adipocytes are consistent with the *in-vivo* findings that Rosi, but not TPhP, induces brite adipogenesis.

Analysis of the TPhP-induced proteome in 3T3 L1 adipocytes

First, we characterized the adipocytes induced by the two PPARγ ligands, Rosi and TPhP, in 3T3 L1 cells, a mouse-derived pre-adipocyte model. 3T3 L1 cells were differentiated using a standard hormone cocktail for 10 days. During differentiation, cells were treated with Vh (0.1% DMSO, final concentration), Rosi (20 μM), or TPhP (20 μM). Rosi, but not TPhP, significantly increased cell number (**Figure S2B**) Rosi and TPhP significantly induced lipid accumulation (**Figure 3A**). Rosi and TPhP induced *Plin1* expression in a PPARγ-dependent manner (**Figure 3B**). Rosi, but not TPhP, induced expression of the brite adipocyte genes *Elovl3* and *Ucp1* in 3T3 L1 cells, and this induction also is PPARγ-dependent (**Figure 3B**). As in primary human adipocytes, only Rosi significantly induced mitochondrial biogenesis and mitochondrial activity (**Figures 3C-D**). Thus, we performed proteomic analyses with differentiated and treated 3T3-L1s. The heatmap in **Figure 4A** shows that Rosi-treated cells expresses a suite of protein that are distinct from Vh- and TPhP-treated cells. TPhP-treated samples cluster and have expression patterns more similar to Vh-treated cells (**Figure 4A**). The list of protein intensities

and results of the differential analysis are presented in Table S2. Rosi highly upregulated CD36, FABP4, and GPD1 (**Figure 4B**), which are involved in fatty acid and glycerol metabolism (Hotamisligil and Bernlohr 2015; Kiskinis et al. 2014). TPhP highly upregulated CNN2, VASP, and SEC13 (**Figure 4B**), which are involved in actin polymerization (Erasmus et al. 2016).

Protein phosphorylation is one of the most common post-translational modifications through which protein function is regulated in response to extracellular stimuli (Ardito et al. 2017); therefore we also investigated the effects of Rosi and TPhP on the phospho-proteome. Rosi differentially regulated phosphorylation sites compared to Vh and TPhP (**Figure 5A**). All phosphorylation sites and results of the differential analysis are listed in Table S3. Rosi highly upregulated the phosphoproteins, SDPR and GYS1 (**Figure 5B**), which are involved in insulin signaling and glucose metabolism (Bugge et al. 2009; Hansson et al. 2017). TPhP highly upregulated the phosphoproteins STEAP3 and EPB41L3 (**Figure 5B**), which are involved in iron metabolism and tumor suppression, respectively (Lambe et al. 2009; Zeng et al. 2018).

We created a combined differential protein and phosphoprotein ranked list to perform enrichment analysis in order to determine which pathways are enriched or shared by the two PPARγ ligands (**Figure 6**). The complete enrichment results are listed in Table S4. **Figure 6** shows a network representation of pathways, where nodes are pathways and edges are shared genes between pathways. Pathways (nodes) significantly enriched by Rosi (red colored nodes), significantly enriched by TPhP (purple colored nodes), or shared by both (nodes split with red and purple). In order to interrogate the role of PPARy in the pathway networks, nodes were highlighted green to indicate PPARγ is in the gene set, showing many pathway clusters relate to PPARy activity. Rosi regulated networks related to oxidation/metabolic processes, mitochondrial proteins, and tissue morphogenesis. TPhP regulated networks related to ubiquitination of proteasomes. Shared networks were related to oxidation/metabolic processes as well as regulation of lipid ketones. That Rosi regulated protein networks related to oxidation/metabolic and mitochondrial processes is consistent with the phenotypic differences in the adipocytes that Rosi and TPhP induce.

Effect of TPhP on PPARγ phosphorylation and its contribution to adipocyte differentiation

The phosphoproteomic experiments did not detect PPARγ and its phosphorylation as it was an untargeted proteomic profiling and PPARγ is not a highly expressed protein. Therefore, we used immunoblotting and a mutant form of PPARγ to investigate how phosphorylation of PPARγ at ser273 differentiates the effects of Rosi and TPhP. 3T3 L1 cells were differentiated using a standard hormone cocktail for 10 days. During differentiation, cells were treated with Vh (0.1% DMSO, final concentration), Rosi (20 μM), or TPhP (20 μM). Rosi significantly reduced phosphorylation of PPARγ at ser273 (**Figure 7A**), which also has been shown by others (Banks et al. 2015; Choi et al. 2010). TPhP did not protect PPARγ from phosphorylation (**Figure 7A**).

CDK5 is known to phosphorylate PPARγ at ser273, therefore we also tested whether inhibition of CDK5 by roscovitine (Rosco) would allow TPhP to induce brite adipocyte gene expression. Treatment of 3T3 L1 cells with Rosco (20 μM), along with Rosi and TPhP, during differentiation modestly decreased lipid accumulation (**Figure S3A**) and did not change white adipocyte gene expression (**Figure 7B, Figure S3B**). However, inhibition of Cdk5 by Rosco significantly increased the ability of TPhP to induce brite adipocyte gene expression (**Figure 7B, Figure S3C**).

Using Swiss 3T3 cells expressing wild-type PPARγ (3T3-WT) or PPARγ with alanine substitute for serine at position273 (3T3-SA), we examined whether a constitutively dephosphorylated

PPARγ would enable TPhP to induce brite adipocyte gene expression. Lipid accumulation was less in 3T3-SA cells than in 3T3-WT cells treated with either Rosi or TPhP (**Figure S4A**) and expression of white adipocyte genes was modestly but not significantly reduced (**Figure 7C, Figure S4B**). However, in 3T3-SA cells, TPhP had greater efficacy in inducing brite adipocyte genes, *Adipoq*, *Ucp1* and *Cidea*, in particular (**Figure 7C, Figure S4C**). In summary, when liganded with TPhP, PPARγ remain phosphorylated at ser273, which limits PPARγ's ability to induce brite adipogenesis.

Discussion:

The environmental metabolism disrupting chemical, TPhP, is a PPARγ ligand that can induce adipocyte differentiation (Cano-Sancho et al. 2017; Kim et al. 2019; Pillai et al. 2014; Tung et al. 2017a). Previous studies have shown using the well-studied and characterized preadipocyte model, 3T3-L1cells, that TPhP increased lipid accumulation and mRNA levels of adipocyte differentiation markers such as *Plin1* (Cano-Sancho et al. 2017; Tung et al. 2017a). However, not study has yet investigated the phenotype of the adipocyte that forms. Brite adipogenesis can impact the ratio of lipid-storing (typical of white adipocytes) to lipid-burning adipocytes (Rosenwald and Wolfrum 2014). Thus, skewing of adipogenesis toward white and away from brite adipogenesis could have consequences on healthful adipocyte function. Indeed, rodents that lack brite adipocytes develop obesity, with insulin resistance and hepatic steatosis (Cohen et al. 2014). Here, we examined the characteristics of TPhP-induced adipocytes in multiple models and examined the mechanism that differentiates TPhP-liganded-PPARγ from Rosi-liganded-PPARγ.

In vivo studies to date have only examined the effect of early life TPhP exposure on adipose and metabolic homeostasis in adulthood (Green et al. 2016; Patisaul et al. 2013; Wang et al. 2018). Further, no other study has yet investigated the effects of TPhP exposure on the browning of white adipose tissue. Inguinal adipose tissue is the largest fat depot that can recruit brite adipocytes upon chronic cold exposure of mice, and mature adipocytes in this depot have the potential to transdifferentiate from cells with the typical characteristics of white adipocytes to characteristics of brown adipocytes (Rosenwald and Wolfrum 2014; Waldén et al. 2012). The reduction of adipocyte size and reduction of adipocyte number in IWAT of TPhP-exposed mice suggests that TPhP induced adipocyte hyperplasia, rather than hypertrophy. However, TPhP failed to induce expression of *Cidea* and significantly reduced the expression of *Elovl3* and *Ucp1* in the mature adipocytes isolated from the IWAT. Thus, it appears that TPhP induces the differentiation of new, white adipocytes in IWAT. Lineage-tracing studies are needed to confirm this hypothesis.

The dose we chose for *in vivo* TPhP exposure (10 mg/kg/day) was to match the dose for Rosi (10 mg/kg) that was previously used to evaluate browning potential of the adipose tissue ((Wang et al. 2016). Our *in vivo* dose is higher than the human average daily intake of triphenyl phosphate among 25-30 year old females (0.8 ng/kg-body weight-per day) and same age group males (1.6 ng/kg-body weight-per day) of 8 population groups in the FDA's monitoring program for chemical contaminants in the U.S. food supply (Gunderson 1988). However, our implemented dose is lower than that of studies that used a dose (70mg/kg/day) from an old *in vivo* TPhP exposure study in male Holtzman rats (Sutton et al. 1960) to derive a non-regulatory reference dose for TPhP (Ali et al. 2012; Li et al. 2018). Our TPhP dose is also in the lower-middle range of recent *in vivo* exposure studies as one recent study exposed C57Bl/6 dams to 0, 5, 25, or 50 mg/kg TPhP via intraperitoneal injection (Philbrook et al. 2018), and National Toxicology Program (NTP) recently exposed male Harlan Sprague Dawley rats to 0, 55, 110, 220, 441, and 881 mg/kg TPHP daily for 4 days by oral gavage (National Toxicology Program 2018). Another important question is whether sex modifies the effect of TPhP exposure. A

recent study reported that perinatal TPhP exposure increased body and fat mass in 3.5 months-old male and female rats, while TPhP exposure increased plasma non-esterified- fasting fatty acids and accelerated type 2 diabetes mellitus onset only in the males (Green et al. 2016). In a future study, we can further validate if we observe similar adipogenic and metabolic effects in female mice from same *in-vivo* exposure methods done in this study.

Like in 3T3-L1 cells and in mice *in vivo*, TPhP fails to induce brite adipocyte differentiation in primary human preadipocytes. In accordance with a previous study (Tung et al. 2017b), TPhP induced lipid accumulation and expression of white adipocyte genes (i.e. *Plin1* and *Cidec*). However, TPhP induced neither brite adipocyte genes such as *Elovl3* and *Ucp1* nor mitochondrial biogenesis or activity in the differentiated primary human adipocytes. Interesting, humans with a lower propensity to develop brite adipocytes are more likely to be obese/diabetic (Claussnitzer et al. 2015; Timmons and Pedersen 2009). Moreover, our combined proteomic and phosphoproteomic analyses reveal that the two PPARγ ligands, Rosi and TPhP, show distinct expression of proteins and enrichment of pathways. Compared to TPhP, Rosi enriched more regulatory networks related to oxidation/metabolic processes and mitochondrial proteins. Our data set also uncovered an array of phosphorylation changes on several key enzymes, such as SDPR and GYS1, involved in lipid and glucose homeostasis; and these key enzymes were only upregulated by the therapeutic PPARγ ligand, Rosi.

Phosphorylation of PPARγ regulates the suite of genes it can transactivate. In obese mice, which have been fed a high-fat diet, Cdk5 becomes activated in adipose tissues and phosphorylates PPARγ at ser273 (Choi et al. 2010). This modification of PPARγ reduces expression of the insulin-sensitizing adipokine, adiponectin, and studies have suggested that Cdk5-mediated phosphorylation of PPARγ may be involved in the pathogenesis of insulin-resistance (Banks et al. 2015; Choi et al. 2010, 2011). The phosphorylation of PPARγ by Cdk5 is blocked by anti-diabetic PPARγ ligands, such as Rosi, and by PPARγ-modifying compounds like Rosco (Banks et al. 2015; Wang et al. 2016). The inhibition of phosphorylation of PPARγ at ser273 improves insulin sensitivity and recently has been linked to browning of adipose (Choi et al. 2010, 2011; Wang et al. 2016). In our *in-vitro* studies with 3T3-L1 cells, we observed that in the presence of TPhP, PPARγ remains phosphorylated at ser273. Further, when PPARγ cannot be phosphorylated at ser273 (either by inhibition of CDK5 or mutation of ser273), TPhP was able to induce brite genes such as *Pgc1a*, *Elovl3*, and *Ucp1*. Interestingly, TPhP gained the ability to induce *Adipoq* expression in 3T3-SA cells; adiponectin is well known to increase insulin sensitivity (Gao et al. 2009; Yadav et al. 2013).

The likely link between the ligand-determined phosphorylation state of PPARγ and the resulting transcriptional repertoire is differential co-regulator recruitment. PPARγ ser273 phosphorylation is regulated by a complex of interacting cofactors and can have downstream effects on the diabetic gene program (Ma et al. 2018). For example, a PPARγ corepressor, NCoR (nuclear receptor corepressor 1), enhances Cdk5 activity on phosphorylating PPARγ ser273, and an *in vivo* study has found that compared to wild type mice fed a HFD, fat-specific NCoR-deficient mice on HFD were prone to obesity yet have enhanced insulin sensitivity (Li et al. 2011). Another study found that Thrap3 (thyroid hormone receptor-associated protein 3) can preferentially interact with PPARγ when ser273 is phosphorylated, and knockdown of Thrap3 in mature adipocytes restored several genes (i.e. adiponectin) dysregulated by Cdk5-mediated PPARγ phosphorylation, without altering adipogenesis (Choi et al. 2014). Hence, in future studies, we can further validate the role of differential recruitment of coregulators upon ligand-activated PPARγ phosphorylation.

Conclusions:

Exposure to the environmental MDC, TPhP, skews adipogenesis toward white adipocytes and away from brite adipocytes. TPhP fails to upregulate expression of genes that contribute to mitochondrial biogenesis and energy expenditure. This is in contrast to the therapeutic PPARγ ligand, Rosi. The mechanism contributing to this discrepancy is likely related to the fact that while Rosi protects PPARγ from phosphorylation at ser273, TPhP fails to do so. Indeed, when PPARγ cannot be phosphorylated, TPhP can much more efficaciously upregulate expression of brite adipocyte genes. Thus, we propose the novel conclusion that TPhP is a selective PPARγ modulator and the basis of that selective modulation is the failure to protect PPARγ from phosphorylation. We hypothesize that this mechanism of selective modulation may explain why a number of other environmental PPARγ ligands (e.g. TBBPA, quinoxyfen, tonalide) also fail to induce brite adipogenesis (Kim et al. 2019). Critical questions remain to be answered, including how exposure to TPhP at environmentally relevant doses in a human-like dietary context influences metabolic homeostasis and how changes in coregulatory recruitment link environmental ligand-induced differences in PPARγ coregulatory recruitment with specific gene repertoires.

References:

Ali N, Dirtu AC, Van den Eede N, Goosey E, Harrad S, Neels H, et al. 2012. Occurrence of alternative flame retardants in indoor dust from New Zealand: indoor sources and human exposure assessment. Chemosphere 88:1276–1282; doi:10.1016/j.chemosphere.2012.03.100.

Ardito F, Giuliani M, Perrone D, Troiano G, Lo Muzio L. 2017. The crucial role of protein phosphorylation in cell signaling and its use as targeted therapy (Review). Int J Mol Med 40:271–280; doi:10.3892/ijmm.2017.3036.

Banks AS, McAllister FE, Camporez JPG, Zushin P-JH, Jurczak MJ, Laznik-Bogoslavski D, et al. 2015. An ERK/Cdk5 axis controls the diabetogenic actions of PPARγ. Nature 517:391–395; doi:10.1038/nature13887.

Belcher SM, Cookman CJ, Patisaul HB, Stapleton HM. 2014. In vitro assessment of human nuclear hormone receptor activity and cytotoxicity of the flame retardant mixture FM 550 and its triarylphosphate and brominated components. Toxicol Lett 228:93–102; doi:10.1016/j.toxlet.2014.04.017.

Bugge A, Grøntved L, Aagaard MM, Borup R, Mandrup S. 2009. The PPARgamma2 A/B-domain plays a gene-specific role in transactivation and cofactor recruitment. Mol Endocrinol 23:794–808; doi:10.1210/me.2008-0236.

Burns KA, Vanden Heuvel JP. 2007. Modulation of PPAR activity via phosphorylation. Biochim Biophys Acta 1771:952–960; doi:10.1016/j.bbalip.2007.04.018.

Cano-Sancho G, Smith A, La Merrill MA. 2017. Triphenyl phosphate enhances adipogenic differentiation, glucose uptake and lipolysis via endocrine and noradrenergic mechanisms. Toxicol In Vitro 40:280–288; doi:10.1016/j.tiv.2017.01.021.

Cantin GT, Shock TR, Park SK, Madhani HD, Yates JR. 2007. Optimizing TiO2-based phosphopeptide enrichment for automated multidimensional liquid chromatography coupled to tandem mass spectrometry. Anal Chem 79:4666–4673; doi:10.1021/ac0618730.

Chandra V, Huang P, Hamuro Y, Raghuram S, Wang Y, Burris TP, et al. 2008. Structure of the intact PPAR-gamma-RXR- nuclear receptor complex on DNA. Nature 456:350–356; doi:10.1038/nature07413.

Chen Y, Pan R, Pfeifer A. 2016. Fat tissues, the brite and the dark sides. Pflugers Arch 468:1803–1807; doi:10.1007/s00424-016-1884-8.

Choi JH, Banks AS, Estall JL, Kajimura S, Boström P, Laznik D, et al. 2010. Anti-diabetic drugs inhibit obesity-linked phosphorylation of PPARγ by Cdk5. Nature 466:451–456; doi:10.1038/nature09291.

Choi JH, Banks AS, Kamenecka TM, Busby SA, Chalmers MJ, Kumar N, et al. 2011. Antidiabetic actions of a non-agonist PPARγ ligand blocking Cdk5-mediated phosphorylation. Nature 477:477–481; doi:10.1038/nature10383.

Choi JH, Choi S-S, Kim ES, Jedrychowski MP, Yang YR, Jang H-J, et al. 2014. Thrap3 docks on phosphoserine 273 of PPARγ and controls diabetic gene programming. Genes Dev 28:2361–2369; doi:10.1101/gad.249367.114.

Claussnitzer M, Dankel SN, Kim K-H, Quon G, Meuleman W, Haugen C, et al. 2015. FTO Obesity Variant Circuitry and Adipocyte Browning in Humans. N Engl J Med 373:895–907; doi:10.1056/NEJMoa1502214.

Cohen P, Levy JD, Zhang Y, Frontini A, Kolodin DP, Svensson KJ, et al. 2014. Ablation of PRDM16 and beige adipose causes metabolic dysfunction and a subcutaneous to visceral fat switch. Cell 156:304–316; doi:10.1016/j.cell.2013.12.021.

Erasmus JC, Bruche S, Pizarro L, Maimari N, Pogglioli T, Tomlinson C, et al. 2016. Defining functional interactions during biogenesis of epithelial junctions. Nat Commun 7:13542; doi:10.1038/ncomms13542.

Fang M, Webster TF, Stapleton HM. 2015. Activation of Human Peroxisome Proliferator-Activated Nuclear Receptors (PPARγ1) by Semi-Volatile Compounds (SVOCs) and Chemical Mixtures in Indoor Dust. Environ Sci Technol 49:10057–10064; doi:10.1021/acs.est.5b01523.

Gao J, He J, Zhai Y, Wada T, Xie W. 2009. The constitutive androstane receptor is an anti-obesity nuclear receptor that improves insulin sensitivity. J Biol Chem 284:25984–25992; doi:10.1074/jbc.M109.016808.

Garcia-Vallvé S, Guasch L, Tomas-Hernández S, del Bas JM, Ollendorff V, Arola L, et al. 2015. Peroxisome Proliferator-Activated Receptor γ (PPARγ) and Ligand Choreography: Newcomers Take the Stage. J Med Chem 58:5381–5394; doi:10.1021/jm501155f.

Green AJ, Graham JL, Gonzalez EA, La Frano MR, Petropoulou S-SE, Park J-S, et al. 2016. Perinatal triphenyl phosphate exposure accelerates type 2 diabetes onset and increases adipose accumulation in UCD-type 2 diabetes mellitus rats. Reprod Toxicol; doi:10.1016/j.reprotox.2016.07.009.

Gunderson EL. 1988. FDA Total Diet Study, April 1982-April 1984, dietary intakes of pesticides, selected elements, and other chemicals. J Assoc Off Anal Chem 71: 1200–1209.

Hansson B, Rippe C, Kotowska D, Wasserstrom S, Säll J, Göransson O, et al. 2017. Rosiglitazone drives cavin-2/SDPR expression in adipocytes in a CEBPα-dependent manner. PLoS ONE 12:e0173412; doi:10.1371/journal.pone.0173412.

Heindel JJ, Blumberg B, Cave M, Machtinger R, Mantovani A, Mendez MA, et al. 2017. Metabolism disrupting chemicals and metabolic disorders. Reprod Toxicol 68:3–33; doi:10.1016/j.reprotox.2016.10.001.

Hong J, Stubbins RE, Smith RR, Harvey AE, Núñez NP. 2009. Differential susceptibility to obesity between male, female and ovariectomized female mice. Nutr J 8:11; doi:10.1186/1475-2891-8-11.

Hotamisligil GS, Bernlohr DA. 2015. Metabolic functions of FABPs--mechanisms and therapeutic implications. Nat Rev Endocrinol 11:592–605; doi:10.1038/nrendo.2015.122.

Hwang L-L, Wang C-H, Li T-L, Chang S-D, Lin L-C, Chen C-P, et al. 2010. Sex differences in high-fat diet-induced obesity, metabolic alterations and learning, and synaptic plasticity deficits in mice. Obesity (Silver Spring) 18:463–469; doi:10.1038/oby.2009.273.

Kalinovich AV, de Jong JMA, Cannon B, Nedergaard J. 2017. UCP1 in adipose tissues: two steps to full browning. Biochimie 134:127–137; doi:10.1016/j.biochi.2017.01.007.

Kim S, Li A, Monti S, Schlezinger JJ. 2018. Tributyltin induces a transcriptional response without a brite adipocyte signature in adipocyte models. Arch Toxicol 92:2859–2874; doi:10.1007/s00204-018-2268-y.

Kim T-H, Kim M-Y, Jo S-H, Park J-M, Ahn Y-H. 2013. Modulation of the transcriptional activity of peroxisome proliferator-activated receptor gamma by protein-protein interactions and post-translational modifications. Yonsei Med J 54:545–559; doi:10.3349/ymj.2013.54.3.545.

Kiskinis E, Chatzeli L, Curry E, Kaforou M, Frontini A, Cinti S, et al. 2014. RIP140 represses the “brown-in-white” adipocyte program including a futile cycle of triacylglycerol breakdown and synthesis. Mol Endocrinol 28:344–356; doi:10.1210/me.2013-1254.

Kojima H, Takeuchi S, Itoh T, Iida M, Kobayashi S, Yoshida T. 2013. In vitro endocrine disruption potential of organophosphate flame retardants via human nuclear receptors. Toxicology 314:76–83; doi:10.1016/j.tox.2013.09.004.

Kojima H, Takeuchi S, Van den Eede N, Covaci A. 2016. Effects of primary metabolites of organophosphate flame retardants on transcriptional activity via human nuclear receptors. Toxicol Lett 245:31–39; doi:10.1016/j.toxlet.2016.01.004.

Lambe T, Simpson RJ, Dawson S, Bouriez-Jones T, Crockford TL, Lepherd M, et al. 2009. Identification of a Steap3 endosomal targeting motif essential for normal iron metabolism. Blood 113:1805–1808; doi:10.1182/blood-2007-11-120402.

Lefterova MI, Haakonsson AK, Lazar MA, Mandrup S. 2014. PPARγ and the global map of adipogenesis and beyond. Trends Endocrinol Metab 25:293–302; doi:10.1016/j.tem.2014.04.001.

Lemkul JA, Lewis SN, Bassaganya-Riera J, Bevan DR. 2015. Phosphorylation of PPARγ Affects the Collective Motions of the PPARγ-RXRα-DNA Complex. PLoS ONE 10:e0123984; doi:10.1371/journal.pone.0123984.

Li J, Zhang Z, Ma L, Zhang Y, Niu Z. 2018. Implementation of USEPA RfD and SFO for improved risk assessment of organophosphate esters (organophosphate flame retardants and plasticizers). Environ Int 114:21–26; doi:10.1016/j.envint.2018.02.027.

Li P, Fan W, Xu J, Lu M, Yamamoto H, Auwerx J, et al. 2011. Adipocyte NCoR knockout decreases PPARγ phosphorylation and enhances PPARγ activity and insulin sensitivity. Cell 147:815–826; doi:10.1016/j.cell.2011.09.050.

Ma X, Wang D, Zhao W, Xu L. 2018. Deciphering the Roles of PPARγ in Adipocytes via Dynamic Change of Transcription Complex. Front Endocrinol (Lausanne) 9:473; doi:10.3389/fendo.2018.00473.

Mendelsohn E, Mendelsohn E, Hagopian A, Hoffman K, Butt CM, Lorenzo A, et al. Nail polish as a source of exposure to triphenyl phosphate. Environment international 86:45–51; doi:10.1016/j.envint.2015.10.005, info:doi/10.1016/j.envint.2015.10.005.

Merico D, Isserlin R, Stueker O, Emili A, Bader GD. 2010. Enrichment map: a network-based method for gene-set enrichment visualization and interpretation. PLoS ONE 5:e13984; doi:10.1371/journal.pone.0013984.

National Toxicology Program. 2018. *NTP Research Report on In Vivo Repeat Dose Biological Potency Study of Triphenyl Phosphate (CAS No. 115-86-6) in Male Sprague Dawley Rats (Hsd: Sprague Dawley SD) (Gavage Studies): Research Report 8*. National Toxicology Program:Durham (NC).

Ospina M, Jayatilaka NK, Wong L-Y, Restrepo P, Calafat AM. 2018. Exposure to organophosphate flame retardant chemicals in the U.S. general population: Data from the 2013-2014 National Health and Nutrition Examination Survey. Environ Int 110:32–41; doi:10.1016/j.envint.2017.10.001.

Paschos GK, Tang SY, Theken KN, Li X, Verginadis I, Lekkas D, et al. 2018. Cold-Induced Browning of Inguinal White Adipose Tissue Is Independent of Adipose Tissue Cyclooxygenase-2. Cell Rep 24:809–814; doi:10.1016/j.celrep.2018.06.082.

Patisaul HB, Roberts SC, Mabrey N, McCaffrey KA, Gear RB, Braun J, et al. 2013. Accumulation and endocrine disrupting effects of the flame retardant mixture Firemaster® 550 in rats: an exploratory assessment. J Biochem Mol Toxicol 27:124–136; doi:10.1002/jbt.21439.

Philbrook NA, Restivo VE, Belanger CL, Winn LM. 2018. Gestational triphenyl phosphate exposure in C57Bl/6 mice perturbs expression of insulin-like growth factor signaling genes in maternal and fetal liver. Birth Defects Res 110:483–494; doi:10.1002/bdr2.1185.

Pillai HK, Fang M, Beglov D, Kozakov D, Vajda S, Stapleton HM, et al. 2014. Ligand binding and activation of PPARγ by Firemaster® 550: effects on adipogenesis and osteogenesis in vitro. Environ Health Perspect 122:1225–1232; doi:10.1289/ehp.1408111.

Qiang L, Wang L, Kon N, Zhao W, Lee S, Zhang Y, et al. 2012. Brown remodeling of white adipose tissue by SirT1-dependent deacetylation of Pparγ. Cell 150:620–632; doi:10.1016/j.cell.2012.06.027.

Rabhi N, Hannou SA, Gromada X, Salas E, Yao X, Oger F, et al. 2018. Cdkn2a deficiency promotes adipose tissue browning. Mol Metab 8:65–76; doi:10.1016/j.molmet.2017.11.012.

Rangwala SM, Rhoades B, Shapiro JS, Rich AS, Kim JK, Shulman GI, et al. 2003. Genetic modulation of PPARgamma phosphorylation regulates insulin sensitivity. Dev Cell 5: 657–663.

Ritchie ME, Phipson B, Wu D, Hu Y, Law CW, Shi W, et al. 2015. limma powers differential expression analyses for RNA-sequencing and microarray studies. Nucleic Acids Res 43:e47; doi:10.1093/nar/gkv007.

Rosenwald M, Wolfrum C. 2014. The origin and definition of brite versus white and classical brown adipocytes. Adipocyte 3:4–9; doi:10.4161/adip.26232.

Schneider CA, Rasband WS, Eliceiri KW. 2012. NIH Image to ImageJ: 25 years of image analysis. Nat Methods 9: 671–675.

Schwartz MW, Seeley RJ, Zeltser LM, Drewnowski A, Ravussin E, Redman LM, et al. 2017. Obesity pathogenesis: An endocrine society scientific statement. Endocr Rev 38:267-296.

Shao D, Rangwala SM, Bailey ST, Krakow SL, Reginato MJ, Lazar MA. 1998. Interdomain communication regulating ligand binding by PPAR-gamma. Nature 396:377–380; doi:10.1038/24634.

Subramanian A, Tamayo P, Mootha VK, Mukherjee S, Ebert BL, Gillette MA, et al. 2005. Gene set enrichment analysis: a knowledge-based approach for interpreting genome-wide expression profiles. Proc Natl Acad Sci USA 102:15545–15550; doi:10.1073/pnas.0506580102.

Sutton WL, Terhaar CJ, Miller FA, Scherberger RF, Riley EC, Roudabush RL, et al. 1960. Studies on the industrial hygiene and toxicology of triphenyl phosphate. Arch Environ Health 1: 33–46.

Timmons JA, Pedersen BK. 2009. The importance of brown adipose tissue. N Engl J Med 361:415–416; author reply 418-421; doi:10.1056/NEJMc091009.

Tung EWY, Ahmed S, Peshdary V, Atlas E. 2017a. Firemaster® 550 and its components isopropylated triphenyl phosphate and triphenyl phosphate enhance adipogenesis and transcriptional activity of peroxisome proliferator activated receptor (Pparγ) on the adipocyte protein 2 (aP2) promoter. PLoS ONE 12:e0175855; doi:10.1371/journal.pone.0175855.

Tung EWY, Peshdary V, Gagné R, Rowan-Carroll A, Yauk CL, Boudreau A, et al. 2017b. Adipogenic Effects and Gene Expression Profiling of Firemaster® 550 Components in Human Primary Preadipocytes. Environ Health Perspect 125:097013; doi:10.1289/EHP1318.

Tyanova S, Temu T, Cox J. 2016. The MaxQuant computational platform for mass spectrometry-based shotgun proteomics. Nat Protoc 11:2301–2319; doi:10.1038/nprot.2016.136.

Waldén TB, Hansen IR, Timmons JA, Cannon B, Nedergaard J. 2012. Recruited vs. nonrecruited molecular signatures of brown, “brite,” and white adipose tissues. Am J Physiol Endocrinol Metab 302:E19-31; doi:10.1152/ajpendo.00249.2011.

Wang D, Yan S, Yan J, Teng M, Meng Z, Li R, et al. 2018. Effects of triphenyl phosphate exposure during fetal development on obesity and metabolic dysfunctions in adult mice: Impaired lipid metabolism and intestinal dysbiosis. Environ Pollut 246:630–638; doi:10.1016/j.envpol.2018.12.053.

Wang H, Liu L, Lin JZ, Aprahamian TR, Farmer SR. 2016. Browning of White Adipose Tissue with Roscovitine Induces a Distinct Population of UCP1(+) Adipocytes. Cell Metab 24:835–847; doi:10.1016/j.cmet.2016.10.005.

Wang Y, Li W, Martínez-Moral MP, Sun H, Kannan K. 2019. Metabolites of organophosphate esters in urine from the United States: Concentrations, temporal variability, and exposure assessment. Environ Int 122:213–221; doi:10.1016/j.envint.2018.11.007.

Yadav A, Kataria MA, Saini V, Yadav A. 2013. Role of leptin and adiponectin in insulin resistance. Clin Chim Acta 417:80–84; doi:10.1016/j.cca.2012.12.007.

Zeng R, Liu Y, Jiang Z-J, Huang J-P, Wang Y, Li X-F, et al. 2018. EPB41L3 is a potential tumor suppressor gene and prognostic indicator in esophageal squamous cell carcinoma. Int J Oncol; doi:10.3892/ijo.2018.4316.

Figure 1

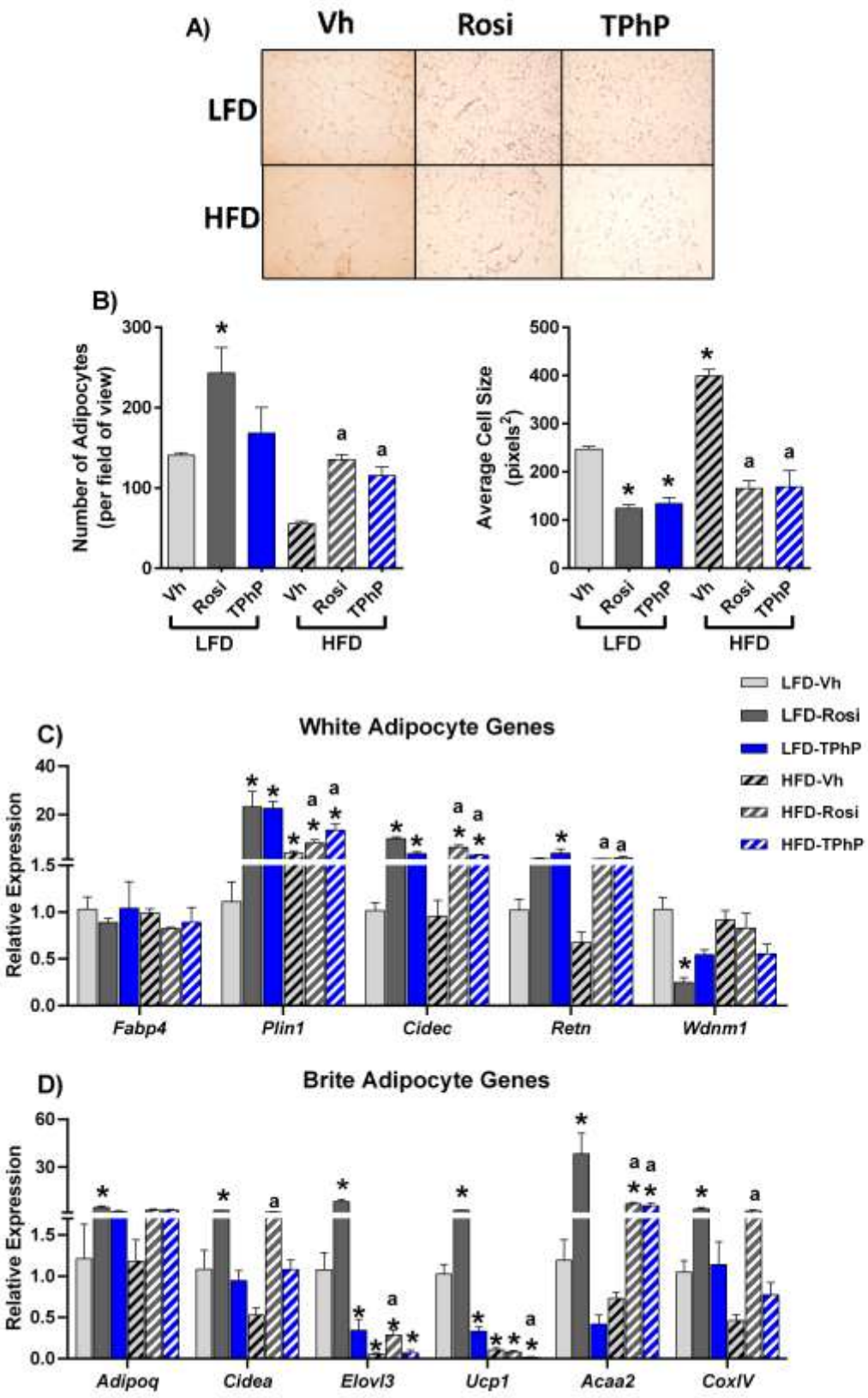

Figure 1. IWAT histology and gene expression in Rosi- and TPhP-treated mice. Six-week-old C57BL/6J male mice were fed either a diet with 10% kcal% fat (LFD) or 60% kcal% fat (HFD) for a total of 13 weeks. Seven weeks after initiation of the diet, mice were i.p., daily for 6 weeks with vehicle, rosiglitazone (10 mg/kg), or triphenyl phosphate (10 mg/kg). Inguinal white adipose tissue (IWAT) was stained with hematoxylin and eosin. **(A)** Representative micrograph. **(B)** The number and size of adipocytes were measured using ImageJ. Mature adipocytes were isolated from IWAT by digestion, filtering and centrifugation. Adipocytes were analyzed for gene expression by RT-qPCR. **(C)** White adipocyte marker genes. **(D)** Brite adipocyte genes. Data are presented as mean $\pm$ SE (n=5). Statistically different from LFD Vh-treated (*$p<0.05$) or HFD Vh-treated ($^{a}p<0.05$, ANOVA, Dunnett's).

Figure 2

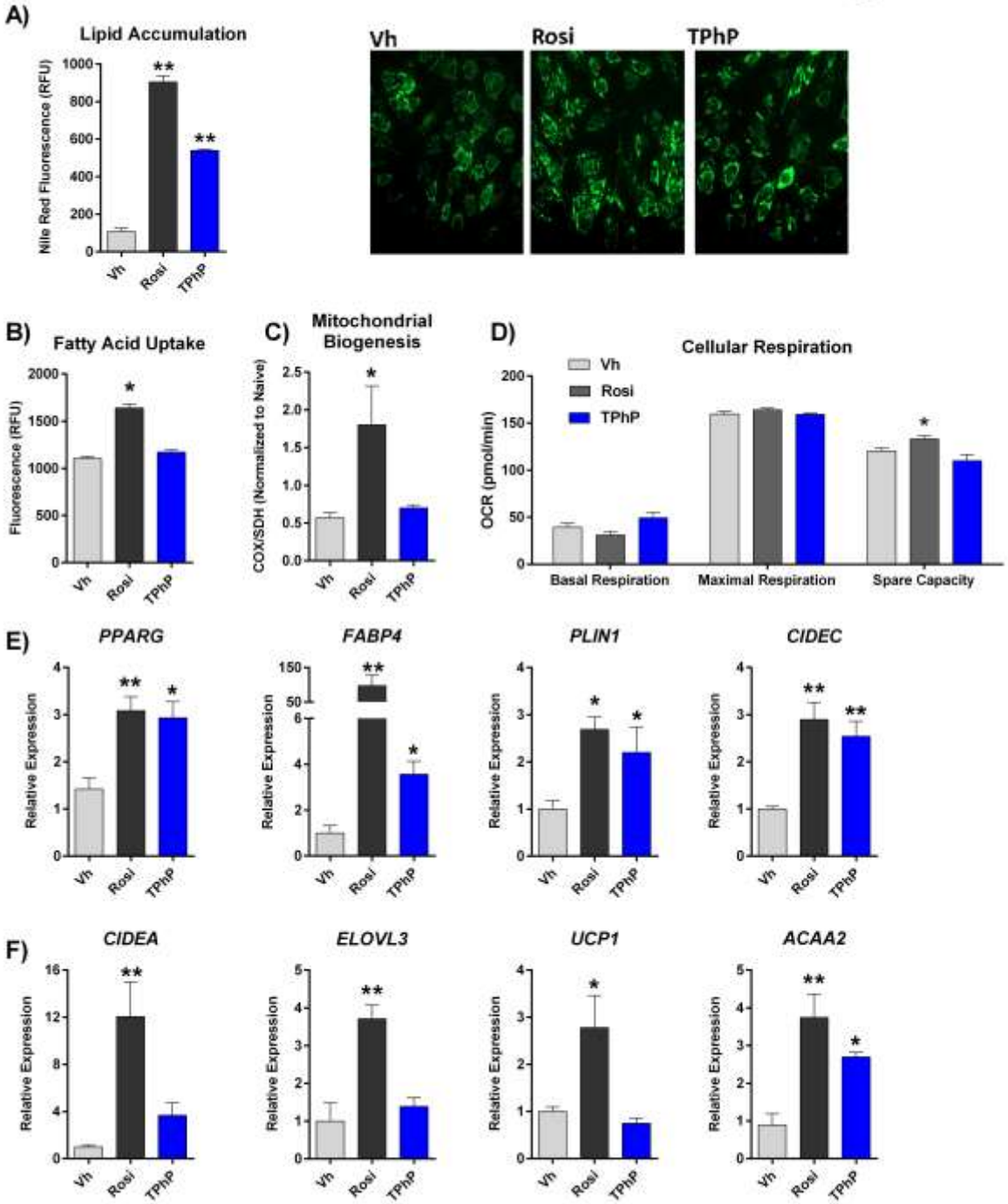

Figure 2. Functions of and gene expression in human adipocytes differentiated with Rosi and TPhP.

Confluent primary human adipocytes were differentiated using a standard hormone cocktail for a total of 14 days. During differentiation, cells were treated with vehicle (0.1% DMSO, final concentration), Rosi (4 μM), or TPhP (4 μM). **(A)** Lipid accumulation was determined by Nile Red staining. **(B)** Fatty acid uptake was analyzed using a dodecanoic acid fluorescent fatty acid substrate. **(C)** Mitochondrial biogenesis was analyzed by measuring mitochondria-specific proteins. **(D)** Cellular respiration was measured using the Seahorse assay. Gene expression was analyzed by RT-qPCR. **(E)** White adipocyte marker genes. **(F)** Brite adipocyte genes. Data are presented as mean $\pm$ SE of adipocytes differentiated from 3 individuals. Statistically different from Vh-treated (*$p<0.05$ or **$p<0.01$, ANOVA, Dunnett's).

Figure 3

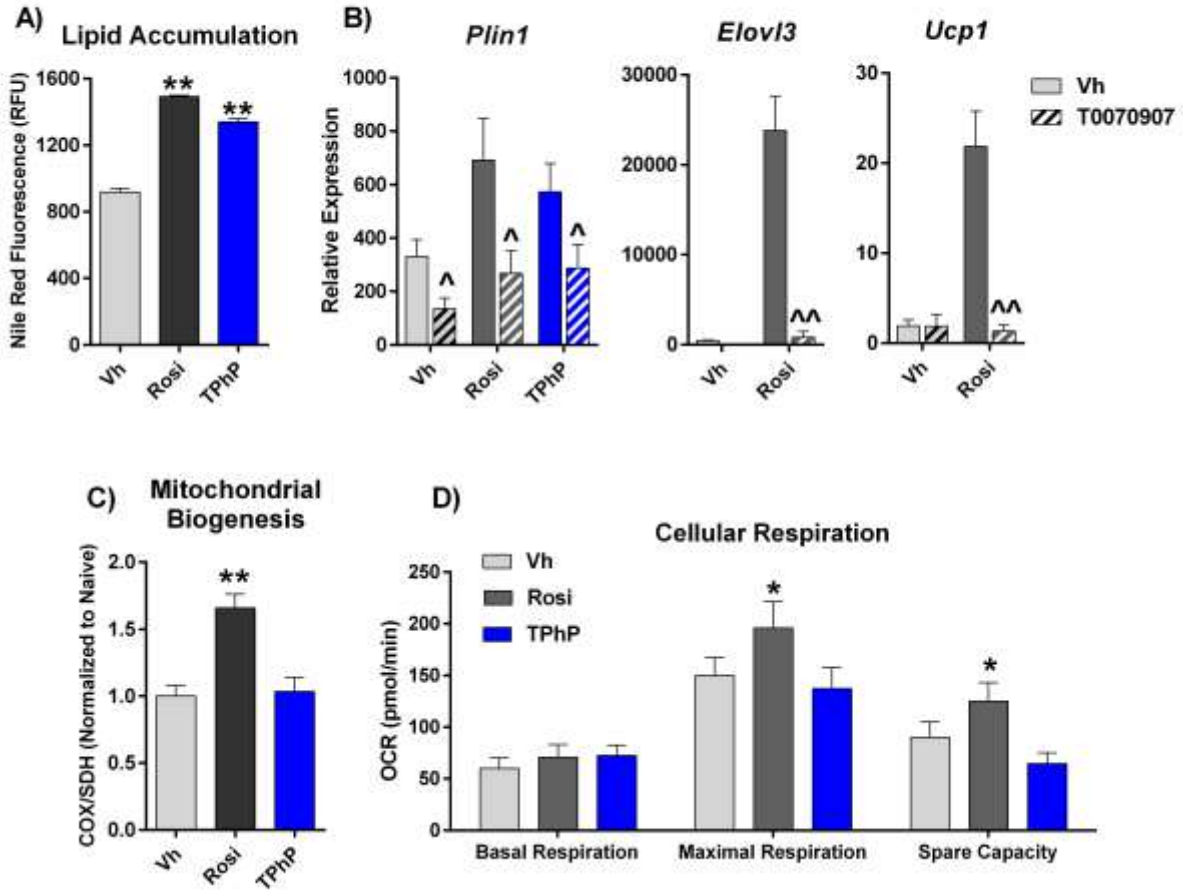

Figure 3. Functions of and gene expression in 3T3 L1 adipocytes differentiated with Rosi and TPhP.

Confluent 3T3 L1 cells were differentiated using a standard hormone cocktail for 10 days. During differentiation, cells were treated with Vh (0.1% DMSO, final concentration), Rosi (20 μM), or TPhP (20 μM) in the presence or absence of the PPARγ antagonist T0070907 (20 μM). **(A)** Lipid accumulation was determined by Nile Red staining. **(B)** Gene expression was analyzed by RT-qPCR. **(C)** Mitochondrial biogenesis was analyzed by measuring mitochondria-specific proteins. **(D)** Cellular respiration was measured using the Seahorse assay. Data are presented as mean ± SE (n=3-6). Statistically different from Vh-treated (*p<0.05 or **p<0.01, ANOVA, Dunnett's).

Figure 4

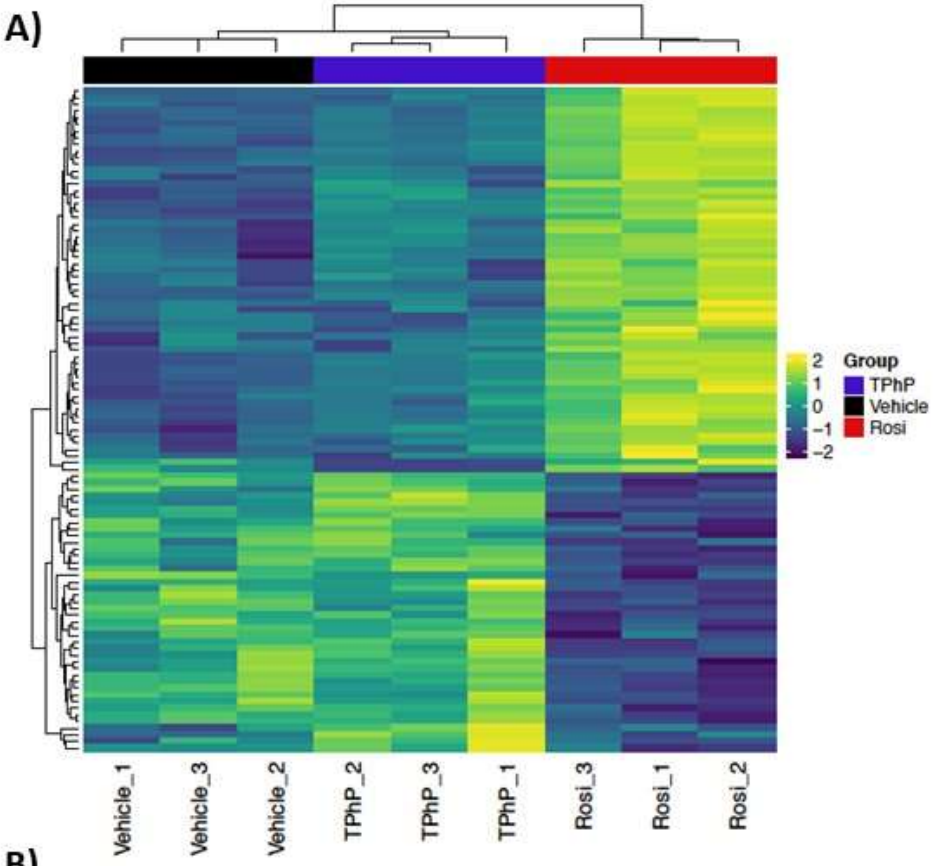

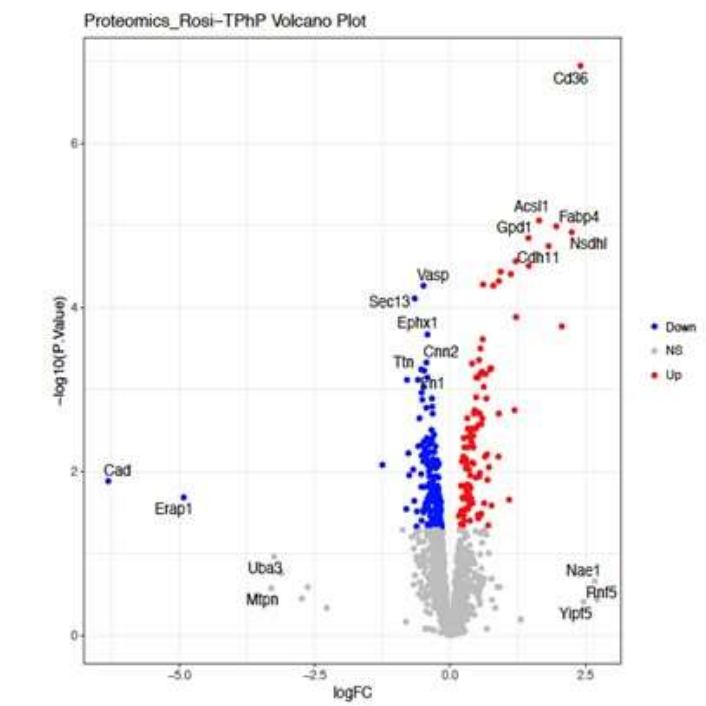

Figure 4. Proteomes of 3T3 L1 adipocytes differentiated with Rosi and TPhP.
Confluent 3T3 L1 cells were differentiated as described in Figure 3. The proteome was analyzed by precision quantitative nanoLC-tandem MS. **(A)** Heatmap and **(B)** volcano plot of top differentially expressed proteins between Rosi and TPhP.

Figure5

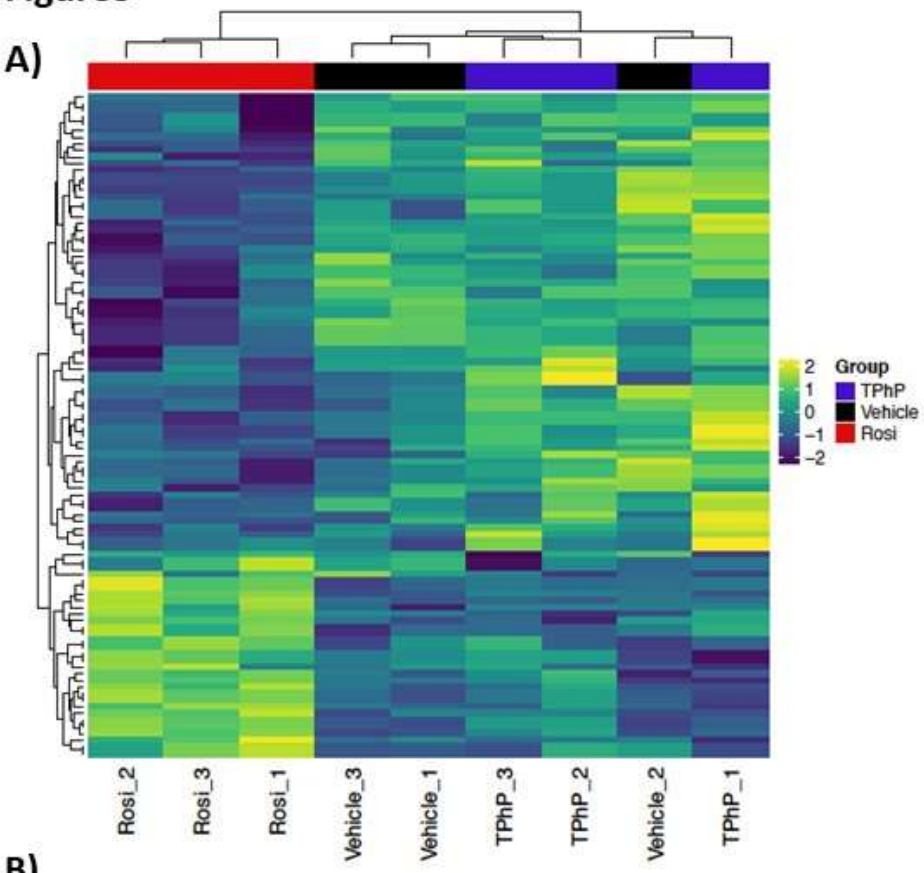

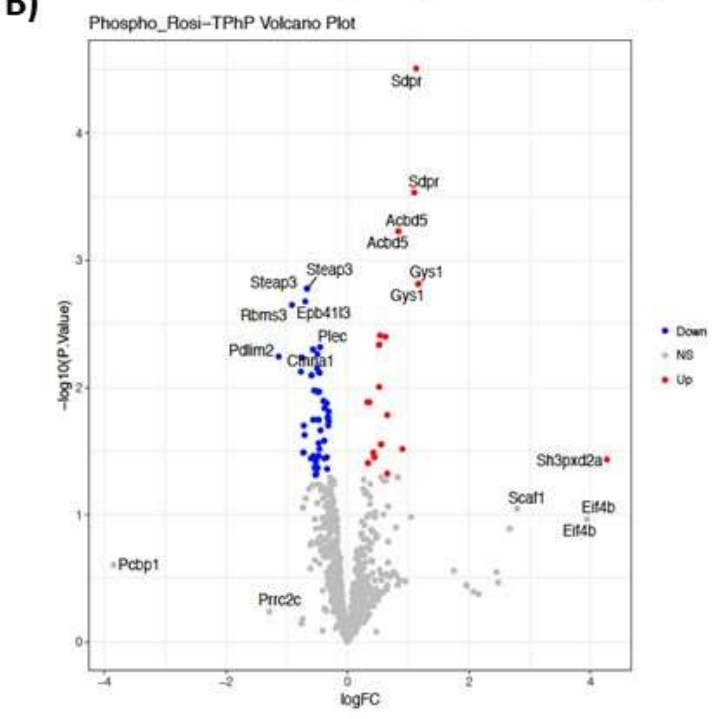

Figure 5. Phosphoproteomes of 3T3 L1 adipocytes differentiated with Rosi and TPhP. Confluent 3T3 L1 cells were differentiated as described in Figure 3. Phospho-peptides were enriched using TiO2 and then analyzed by precision quantitative nanoLC-tandem MS. **(A)** Heatmap and **(B)** volcano plot of top differentially expressed phospho-proteins between Rosi and TPhP.

Figure 6

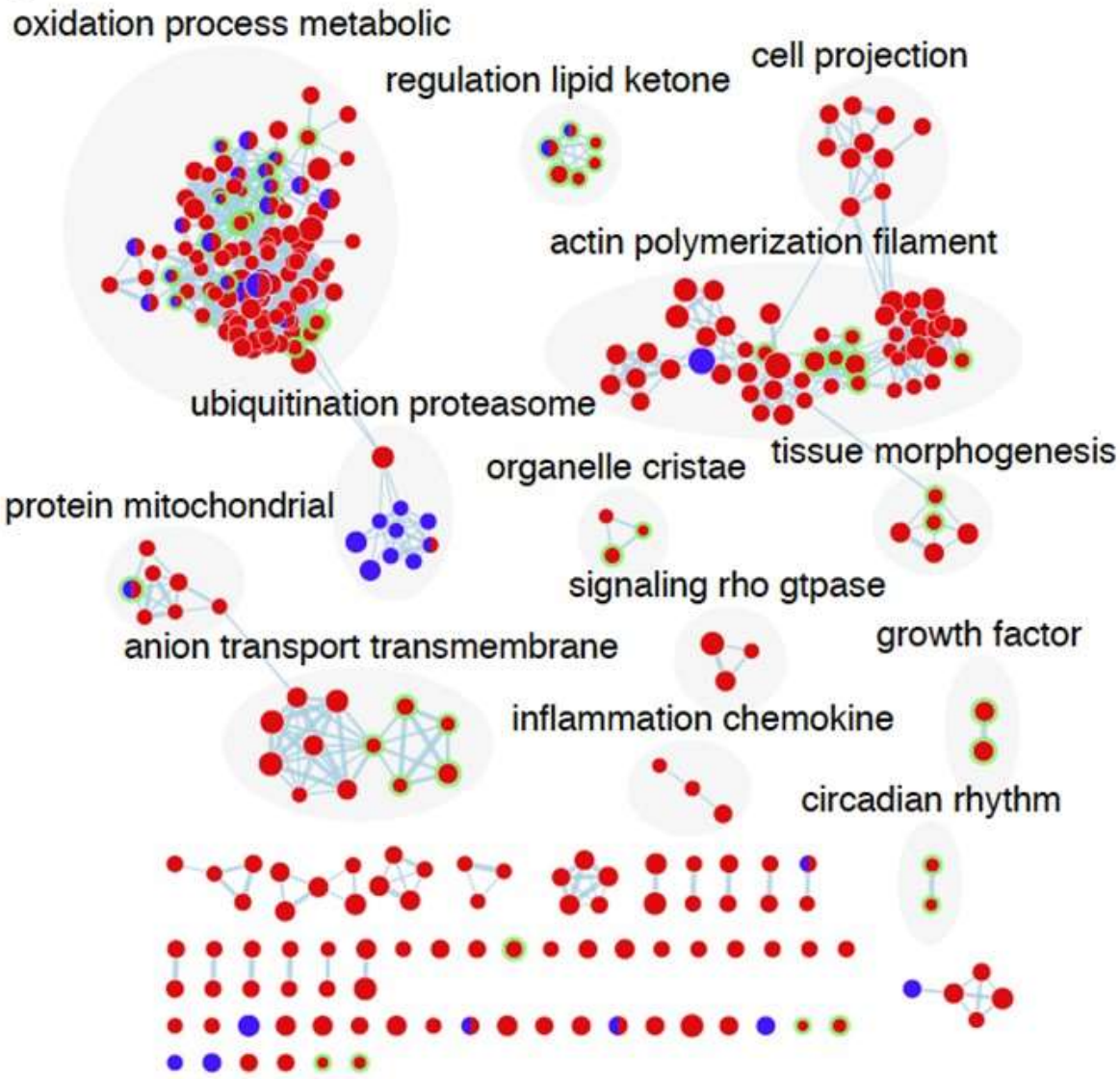

Legend:

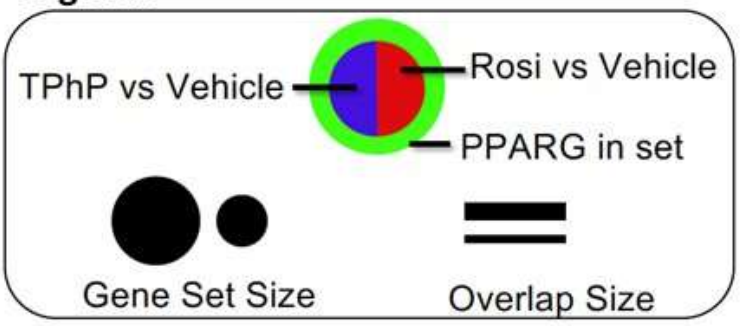

Figure 6. Network analyses of Rosi and TPhP-induced proteomes.
Pathway themes are displayed above highlighted clusters. Nodes in red indicates enriched pathways in Rosi, blue indicates enriched pathways by TPhP, red/blue indicates shared pathways between Rosi and TPhP. Nodes with green surrounding indicate the presence of PPARγ in the pathway set.

Figure 7

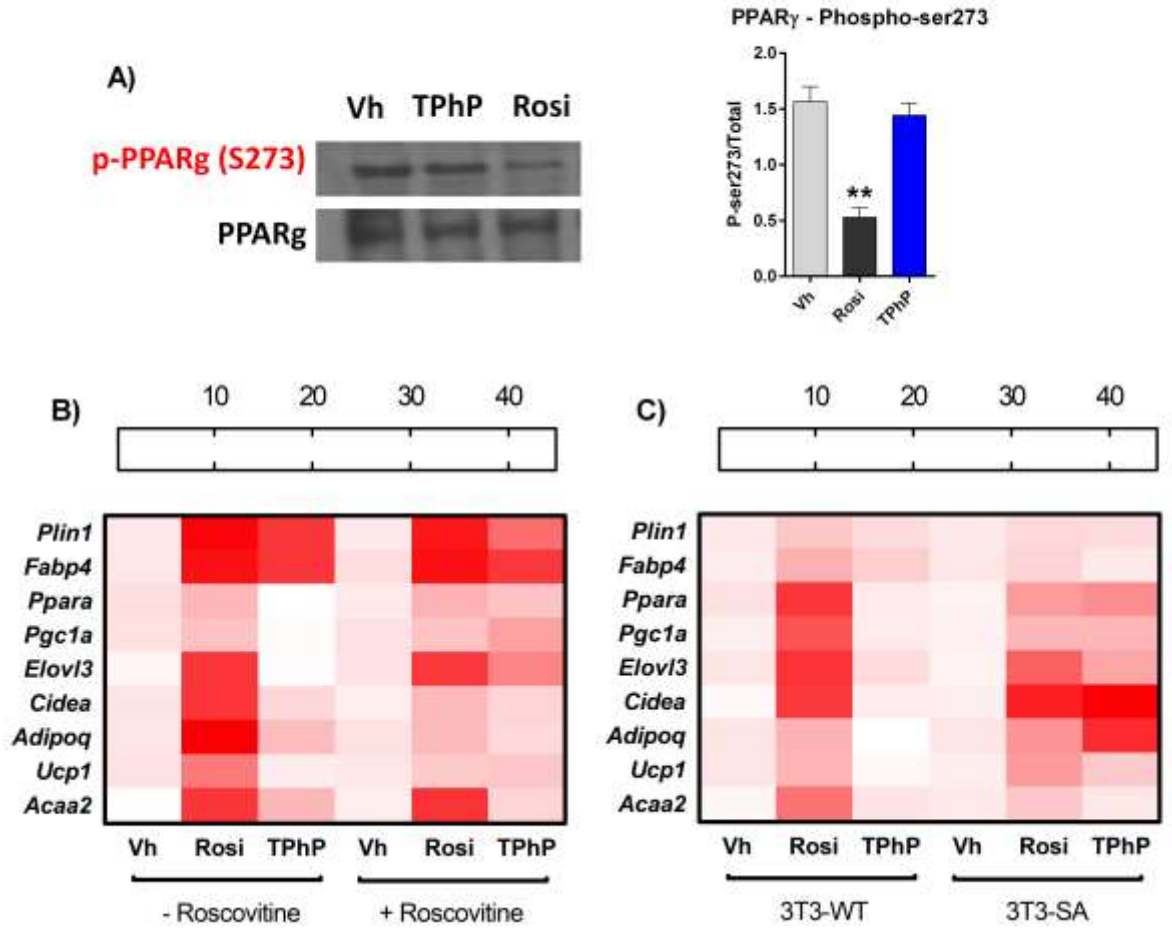

Figure 7. PPARγ phosphorylation and its effect on gene expression adipocytes differentiated with Rosi and TPhP.

(A) Confluent 3T3 L1 cells were differentiated as described in Figure 3 and phosphorylation of PPARγ at ser273 was determined relative to total PPARγ by immunoblot. **(B)** Confluent 3T3 L1 cells were differentiated as described in Figure 3, in the presence or absence of roscovitine (Rosco, 20 μM). Gene expression was determined by RT-qPCR and presented as a heatmap of expression levels of white adipocyte markers (*Plin1, Fabp4*) and brite adipocyte markers (*Ppara, Pgc1a, Elovl3, Cidea, Adipoq, Ucp1, Acaa2*). **(C)** Confluent 3T3 cells expressing wildtype PPARγ (3T3-WT) or PPARγ with alanine substituted for serine 273 (3T3-SA) were differentiated as described for 3T3 L1 cells in Figure 3. Gene expression was determined by RT-qPCR and presented as a heatmap of expression levels of white and brite adipocyte markers. Data are presented as mean $\pm$ SE ($n \geq 3$). Statistically different from Vh-treated (*$p<0.05$ or **$p<0.01$, ANOVA, Dunnett's).